Catena 214 (2022) 106286

Contents lists available at ScienceDirect

Catena

journal homepage: www.elsevier.com/locate/catena

Physical structure and rainfall controls on subsurface hydrological connectivity in hillslope-riparian-stream continuums

H.B. Xiao [a,1], K. Xu [a,1], Y.M. Zhan [a], J. Wang [a], Z. Wang [a], L. Wang [a], Z.H. Shi [a,b,*]

[a] State Environmental Protection Key Laboratory of Soil Health and Green Remediation, Wuhan 430070, China
[b] CAS Center for Excellence in Quaternary Science and Global Change, Xi'an 710061, China

ARTICLE INFO

Keywords:
Hillslope-riparian-stream continuum
Hydrological connectivity
Physical structure
Rainfall characteristics
Subsurface flow

ABSTRACT

The hydrological connectivity of hillslope-riparian-stream (HRS) continuums is crucial for runoff generation and solute transport. The achievement of water resource protection and water quality improvement requires a systematic understanding of the structure and rainfall controls on HRS connectivity. Herein, two HRS continuums with different soil depths and slopes (HRS-1: thin soil depth and steep slope; HRS-2: thick soil depth and gentle slope) were established. We monitored the soil moisture from the surface to the soil-bedrock interface at 15 min intervals from March to June 2021. The HRS connectivity was analyzed based on soil saturation conditions, and partial least squares regression (PLSR) was used to reveal the relationships between rainfall and HRS connectivity. The results showed that the time required to establish hydrological connectivity in HRS-1 was shorter than that in HRS-2, which indicated that the contribution to runoff of the HRS continuum with a thin soil depth and steep slope was dominant during the early stage of rainstorm. As rainfall intensity increased, the required time was shortened exponentially due to the changes in hydrological connectivity patterns. In addition, the higher connectivity strength (i.e., the magnitude of HRS connectivity) was observed in the HRS-2 than that in the HRS-1 during heavy rainfall events. The PLSR analysis showed that rainfall amount, 30 min maximum rainfall intensity, 15 min maximum rainfall intensity, and rainfall duration were important controls affecting connectivity strength. Rainfall amount and peak rainfall intensity exerted more important effects than did antecedent soil moisture on the connectivity strength. Furthermore, there was a clear rainfall threshold for HRS connectivity, from 14.8 mm in HRS-1 to 21.1 mm in HRS-2. The increased soil depth and reduced slope enhanced the rainfall threshold of HRS connectivity. Our results indicate that the physical structure of the HRS continuum exerts a primary control on the rainfall threshold.

1. Introduction

The hydrological connectivity of the hillslope-riparian-stream (HRS) continuum provides a linkage between the catchment upland and the aquatic environment, and this link is critical for the transport of runoff and solutes from terrestrial landscapes to streams (Detty and McGuire, 2010; Hagedorn et al., 2000; Outram et al., 2016). The HRS connectivity can be established by surface runoff and subsurface flow. Saturated overland flow occurs in only a small part of the forested catchment due to the high soil water infiltration and storage capacity (Rinderer et al., 2019), and shallow subsurface flow is the main runoff contributor (Cartwright and Morgenstern, 2018; Onda et al., 2001). Subsurface flow generally results from the development of saturation above an impeding layer (e.g., the interface of soil and bedrock) and the lateral transport of water through this saturated layer (Fiori and Russo, 2007). This onset of lateral subsurface flow from the hillslope to the stream results in hydrological connectivity between the hillslope and the stream (Blume and van Meerveld, 2015). Thus, an improved understanding of how subsurface saturated flow develops and evolves in time and space is key to elucidating the dynamics of HRS connectivity.

In recent decades, many efforts have been made to describe the subsurface hydrological process (Garvelmann et al., 2012; Stieglitz et al., 2003), while the determination of subsurface saturated flow remains a challenging task due to its unobservability and high spatio-temporal variability. Hillslope trenches (van Verseveld et al., 2009), soil moisture measurements (Han et al., 2020; Nanda et al., 2019),

* Corresponding author at: State Environmental Protection Key Laboratory of Soil Health and Green Remediation, Wuhan 430070, China.
E-mail address: shizhihua70@gmail.com (Z.H. Shi).
[1] Both authors contributed equally to this work and should be considered co-first authors.

https://doi.org/10.1016/j.catena.2022.106286
Received 3 December 2021; Received in revised form 4 March 2022; Accepted 2 April 2022
Available online 8 April 2022

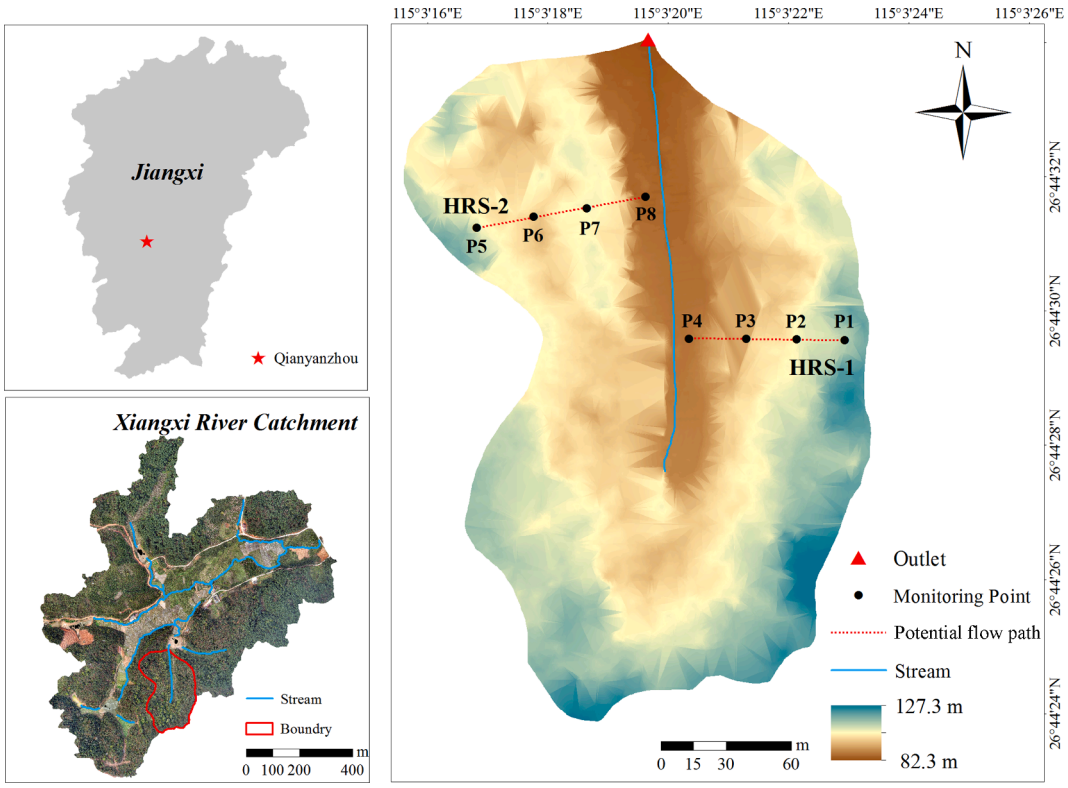

Fig. 1. The location of the study site.

groundwater level monitoring (Ocampo et al., 2006), plot-scale tracer experiments (McGuire and McDonnell, 2010; Weiler and Naef, 2003), and streamflow and chemistry measurements (Burns et al., 2016) have been applied in different contexts to determine subsurface flow or connectivity conditions. Hillslope trench may be one of the most direct ways to measure the subsurface flow, while its installation and maintenance are time-consuming (Blume and van Meerveld, 2015). Furthermore, flow monitoring at a trench may only clarify the hydrological process of a localized region, which makes it difficult to identify the expansion and contraction of runoff source areas (Han et al., 2020; Hopp and McDonnell, 2009). In contrast, distributed soil moisture monitoring can reflect the spatial pattern of soil saturation, which provides the opportunity to observe and quantify subsurface flow pathways (Gish et al., 2005). Furthermore, with the development of field monitoring technology, we can implement the real-time monitoring of soil moisture on scales of minutes or even seconds (Strohmeier et al., 2013). High-frequency and distributed monitoring of soil moisture is therefore regarded as an acceptable and promising method to identify HRS connectivity (Blume and van Meerveld, 2015).

The establishment and extent of HRS connectivity are controlled by physical structures (e.g., soil type, soil depth, and surface and bedrock topography), watershed antecedent conditions (e.g., antecedent soil moisture), and driving forces (e.g., rainfall) (Detty and McGuire, 2010; Han et al., 2020; Hopp and McDonnell, 2009). Over the past decades, extensive progress has been made in identifying the physical structure and rainfall controls on HRS connectivity (Detty and McGuire, 2010; Jencso et al., 2009). For instance, Jencso et al. (2009) found the persistence time of HRS connectivity was positively correlated with the upslope accumulated area. van Meerveld et al. (2015) emphasized the role of bedrock topography on the subsurface flow pathway. The authors concluded that the direction of the subsurface flow path followed the bedrock topography when the groundwater level was low and the overall surface topography when the water level was high. However, Hopp and McDonnell (2009) argued that, except for bedrock topography, researchers should pay more attention to the slope gradient and soil depth when analyzing the subsurface hydrological responses. The changes in slope gradient and soil depth may have significant impacts on the connectivity strength (i.e., the magnitude of HRS connectivity) and the time required to establish hydrological connectivity by altering rainfall infiltration, water storage, and subsurface flow transport. Except for physical structure, rainfall defined as a key driving force also exert significant influences on HRS connectivity. Han et al. (2020) found that rainfall intensity determined the initiation of connectivity and that the time required to establish HRS connectivity decreased exponentially with increasing rainfall intensity. Hillslopes are generally not connected to the streams during rainfall events with a limited rainfall intensity and amount, while runoff-contributing areas can expand upslope with increases in rainfall amount and soil water storage (Han et al., 2020). Numerous studies indicated that the response of subsurface runoff to rainfall was nonlinear in hillslopes (Farrick and Branfireun, 2014; McGuire and McDonnell, 2010), and an obvious threshold behavior was observed in subsurface flow (Tromp-Van Meerveld and McDonnell, 2006). Then, is there a clear rainfall threshold for HRS connectivity? How does this threshold value change with HRS physical structure? These questions need to be further explored.

To clarify the influences of physical structures on HRS connectivity and quantify the relationships between HRS connectivity and rainfall, high-frequency soil moisture monitoring was conducted on two HRS continuums with different soil depths and slopes. A total of 252,000 pieces of soil moisture data were obtained, and 24 rainfall events were recorded from March to June 2021. The time required to establish HRS connectivity and the connectivity strength were analyzed for each rainfall event. The following hypotheses were tested: (1) hydrological connectivity can be established quickly in the HRS continuum with a steeper slope and thinner soil depth; and (2) the HRS connectivity has a clear rainfall threshold which changes with the HRS physical structure. This study provides a better understanding of runoff generation and solute transport by revealing the structure and rainfall controls affecting HRS connectivity.

Table 1
The installation depth of TDR prober in eight soil pits.

Pits	Installed depth (cm)					HRS	Zones	Vegetation	Soil depth (cm)	Elevation (m)	Slope (°)	WSC (mm)
P1	20	40	60	90	–	HRS-1	Upslope	*P. massoniana Lamb. and Michelia L.*	90	117.1	14.5	314.7
P2	10	20	40	–	–	HRS-1	Midslope		40	115.3	10.4	106.2
P3	10	35	55	90	–	HRS-1	Downslope		103	103.5	9.5	276.8
P4	20	50	95	160	–	HRS-1	Riparian	*C. sinensis Osb.*	182	101.7	6.5	406.3
P5	20	40	60	100	–	HRS-2	Upslope	*C. bodinieri Levl. and P. massoniana Lamb.*	105	111.2	8.9	395.9
P6	20	55	80	110	–	HRS-2	Midslope		180	108.3	9.2	504.3
P7	20	50	80	150	–	HRS-2	Downslope		181	105.6	6.7	545.8
P8	20	50	80	130	150	HRS-2	Riparian	*C. sinensis Osb.*	212	102.5	6.4	576.6

WSC represents water storage capacity.

2. Materials and methods

2.1. Site description

Qianyanzhou Ecology Station is located in the Jitai Basin, Taihe County, Jiangxi Province (115°04′13″ E, 26°44′48″ N) and is one of the basic stations of the Chinese Ecosystem Research Network (CERN). This area is influenced by the subtropical monsoon climate, which can be divided into a warm and wet summer monsoon and a cold and dry winter monsoon. The mean annual precipitation is approximately 1540 mm, and approximately 80% is concentrated between April and September (Zhao et al., 2019). The annual evapotranspiration is approximately 1114.8 mm. The temperature varies between −5.9 ℃ and 36.8 ℃, with a mean annual temperature of 16.5 ℃.

The study site is a subcatchment of the Xiangxi River watershed (Fig. 1), which is located near the Qianyanzhou Ecology Station. The area of the subcatchment is approximately 4.74 ha, and the riparian zone accounts for 12.1% of the total watershed area. The digital elevation model (DEM) of the subcatchment (0.3 m resolution) was generated using airborne LiDAR data (Digital Green Earth Technology Co., Ltd., Beijing, China). The elevation ranges between 82.3 m and 127.3 m above sea level, with an average elevation of 102.2 m. Land-use types include forestland and orchard. Orchard planted with navel orange is mainly distributed in the riparian zone, and the planting density and tree age are 1250 stems ha^{-1} and 15 years, respectively. *P. massoniana Lamb.* and *C. bodinieri Levl.* planted in 1985 are the dominant tree species of the forestland. The soil parent material consists of sandstone, sandy conglomerate, and mudstone (Jia and Gao, 2017). The soil type is mainly red loam, classified as oxisol according to the USDA Soil Taxonomy.

2.2. Hillslope-riparian-stream continuums

To clarify the impacts of physical structure on HRS connectivity, two HRS continuums (HRS-1 and HRS-2) were established in the subcatchment with directions nearly perpendicular to the stream (Fig. 1). The HRS continuums were similar in terms of vegetation, parent material, and slope length whereas different in terms of slope gradient and soil depth. Each continuum contains a riparian zone and a planar hillslope, of which the hillslope was further divided into three zones of equal length, including upslope, midslope, and downslope. The slope gradient of the HRS continuums was measured using a geological compass. In HRS-1, the slope gradient of hillslope ranges from 9.5° to 14.5°, with an average value of 11.5° (Table 1). In HRS-2, the slope gradient of hillslope varies between 6.7° and 9.2° and the average slope is 8.3° (Table 1). *Pinus massoniana Lamb.* and *Michelia maudiae Dunn* are the dominant vegetation types on the hillslope of HRS-1. *Pinus massoniana Lamb.* and *Cinnamomum camphora (L.) Presl* are the main vegetation types on the hillslope of HRS-2. *Citrus sinensis Osbeck* was dominated in the riparian zone of both HRS continuums.

One monitoring point was selected in the riparian zone at a distance of approximately 3 m from the stream. Furthermore, a monitoring point was selected near the middle position of each zone in hillslopes (Yang et al., 2014). The selected monitoring points were at least 1 m away from the trees, and the surface topography of monitoring points did not exhibit obvious convex and concave characteristics. In HRS-1, the distances from the monitoring point in the upslope, midslope, downslope, and riparian zones to the stream were 56 m, 39 m, 26 m, and 3 m,

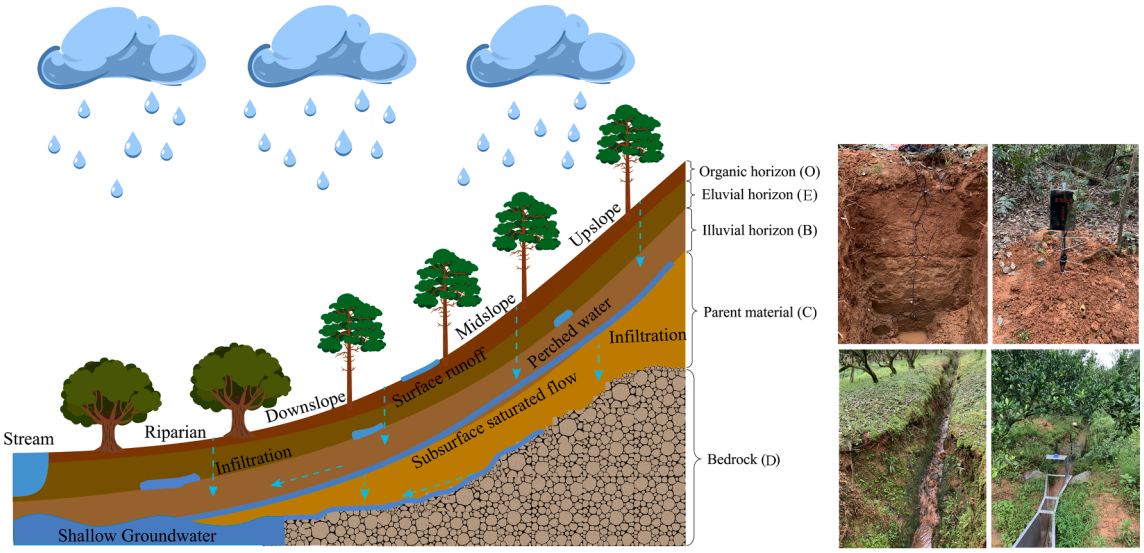

Fig. 2. The schematic diagram of subsurface flow in HRS continuum.

Table 2
The descriptions of rainfall events during the monitoring period.

Events	Date	Rainfall amount (mm)	Duration (h)	I_{mean} (mm/h)	I_{30} (mm/30 min)	ASI-P3 (mm)	ASI-P7 (mm)	API-3 (mm)	API-5 (mm)
1–4	5/18	114.4	66.17	1.73	12.10	237.6	512.2	30.8	31.5
2–1	6/3	61.5	22.17	2.77	18.80	239.2	510.6	0	13.8
3–2	5/7	57.7	24.00	2.40	13.10	212.9	477.0	5.3	22.4
4–5	5/27	44.5	14.67	3.03	8.20	236.0	504.5	5.9	10.3
5–3	5/4	32.4	16.25	1.99	12.9	207.6	469.2	0.2	0.2
6–10	5/11	27.6	24.75	1.12	5.70	224.1	496.8	9.0	9.8
7–13	4/14	27.1	14.33	1.89	4.70	199.0	429.3	4.8	14.6
8–14	5/29	21.3	18.33	1.16	4.30	227.6	511.2	33.5	34.4
9–16	4/18	21.1	41.18	0.51	2.70	209.3	440.4	0.9	20.4
10–15	4/27	19.6	33.00	0.59	3.10	213.4	468.0	9.6	9.6
11–7	5/11	18.8	9.67	1.94	6.50	216.5	497.8	16.3	39.9
12–22	5/24	14.8	22.83	0.65	0.90	225.4	509.2	18.2	66.6
13–18	4/10	14.3	19.66	0.73	1.90	186.7	416.9	10.0	10.3
14–9	6/11	13.8	35.75	0.39	6.10	219.7	498.1	0.4	0.4
15–6	4/7	10.2	5.25	1.94	7.50	180.2	414.1	1.0	1.8
16–8	5/6	9.2	7.08	1.30	6.30	217.4	494.5	0.8	9.4
17–12	4/24	9.1	8.50	1.07	5.00	208.4	465.4	0	4.9
18–11	6/1	5.5	0.67	8.21	5.40	244.7	509.5	16.1	17.9
19–21	4/12	3.6	3.00	1.20	1.10	201.3	425.8	13.8	21.4
20–17	4/28	3.5	1.50	2.33	2.10	218.6	477.0	18.0	24.0
21–23	4/15	2.9	2.83	1.02	0.90	221.5	433.6	27.5	37.1
22–20	5/31	2.7	5.83	0.46	1.30	235.5	518.2	18.2	47.6
23–19	4/11	1.9	1.00	1.90	1.80	200.5	425.4	14.7	21.7
24–24	4/16	1.1	5.75	0.19	0.40	213.0	433.4	23.1	25.6

I_{mean} is the mean rainfall intensity; I_{30} is the 30 min maximum rainfall intensity; ASI-P3 and ASI-P7 are the antecedent soil moisture index in the P3 and P7 pits, respectively. Furthermore, API-3 and API-5 are the antecedent precipitation index for 3 and 5 days, respectively.

respectively. In HRS-2, the distances from the monitoring point in the upslope, midslope, downslope, and riparian zones to the stream were 54 m, 38 m, 25 m, and 3 m, respectively. The HRS continuum was simplified as a point-line topology (Zuecco et al., 2019), in which the point represented the monitoring point and the line between the points indicated the potential flow path (Fig. 1). A soil pit (1.5 m length × 1.5 m width) was excavated in each monitoring point (P1-P8), and soil depth data was acquired by both excavating soil pits (n = 8) and manual drilling (n = 46). The soil depth in the HRS-1 ranged from 40 cm to 182 cm, with an average value of 103.8 cm. In HRS-2, the soil depth varied between 105 cm and 212 cm and the average soil depth is 169.5 cm across the continuum. Soil depth increased sharply in the areas adjacent to the riparian zone. According to the soil color, gravel content, and weathering degree, each soil profile was divided into the following horizons: an upper organic horizon (O, together with humus horizon Ah), a strongly weathered eluvial horizon (E), an enriched illuvial horizon (B), parent material (C), and bedrock (D). In the riparian zone, the B horizon was further divided into an upper strongly illuvial B1 and a lower partially illuvial B2. One or two soil cores (5 cm in height, 5 cm in diameter, and 100 cm^3 in volume) were collected from each soil horizon. A total of 78 undisturbed soil cores were obtained from the eight excavated soil pits. The soil hydraulic conductivity (K_s) of the soil cores was measured with a falling head device using the method of Yu et al. (2014), and the bulk density and saturated moisture content were measured by the drying method. Soil texture was measured using a laser diffraction particle size analyzer (MS-3000, Malvern, UK), and water storage capacity (WSC) was estimated according to Ilek et al. (2017).

The soil texture of the HRS continuums can be classified as sandy clay loam and clay loam (Table S1). The bulk density increased with soil depth at the P3-P8 pits, while the maximum bulk density was observed in the surface soil (0–20 cm) at the P1-P2 pits. The saturated moisture content ranged from 22.44% to 44.88%, showing a decreasing trend with soil depth. Furthermore, the K_s varied between 8.47×10^{-6} mm s^{-1} and 3.95×10^{-2} mm s^{-1}, and the K_s of surface soil (0–20 cm) was almost an order of magnitude larger than that of the deep soil (20–150 cm). The higher K_s was observed in the riparian zone than that in the upslope, midslope, and downslope zones (Table S1). The WSC in the riparian zone was 1.06–3.83 times higher than that in the upslope, midslope, and downslope zones, and the WSC observed in the HRS-2 was higher than that observed in the HRS-1 (Table 1).

2.3. Hydrometric monitoring

The soil volumetric water content was measured in the eight pits (P1-P8) using time domain reflectometry sensors (TDR, S-SMC-M005, Onset Computer Corporation, Bourne, MA, USA) (Fig. 2). The installation depths of the TDR sensors were at the interfaces of adjacent soil horizons. In the P2 pit with a thin soil depth, the installation depth of 40 cm represented the soil–bedrock interface. In the P4, P7, and P8 pits near the stream, the excavated soil depth did not reach the bedrock due to the appearance of shallow groundwater. The soil moisture was monitored at 15 min intervals from March to June 2021. A total of 252,000 pieces of soil moisture data were obtained from 32 TDR sensors.

The rainfall was measured by a tipping bucket rain gauge with an automatic recorder (Texas Electronics TR-525 M), which was installed at the open area approximately 500 m from the catchment outlet. The rainfall monitoring resolution was 0.1 mm, and the monitoring time interval was 5 min. During the monitoring period, a total of 24 rainfall events were recorded, and the total rainfall amount was 568.8 mm (Fig. S1, Table 2). According to the method of Han et al. (2020), we adopted a two-digit ranking method to identify rainfall events (Table 2). The first digit is the ranking of rainfall amount, and the second digit is the ranking of the 30 min maximum rainfall intensity (I_{30}). For example, event 2–1 had the second highest total rainfall amount and the highest rainfall intensity. For each rainfall event, we calculated the rainfall amount, duration, average rainfall intensity (I_{mean}), 15 min maximum rainfall intensity (I_{15}), I_{30}, and antecedent precipitation index (API) (Moreno-de-las-Heras et al., 2020). The antecedent soil moisture index (ASI) was calculated according to Fu et al. 2013:

$$ASI = \sum_{i}^{N} [sm_i \times (dep_i - dep_{i-1})] \quad (1)$$

where N is the number of soil layers, and sm_i is the measured soil moisture at depth i (m^3/m^3); dep_i and dep_{i-1} are the different soil depths (mm). For example, in the P3 pit, dep_1 to dep_4 represent 100, 350, 550, and 900 mm, respectively ($dep_0 = 0$).

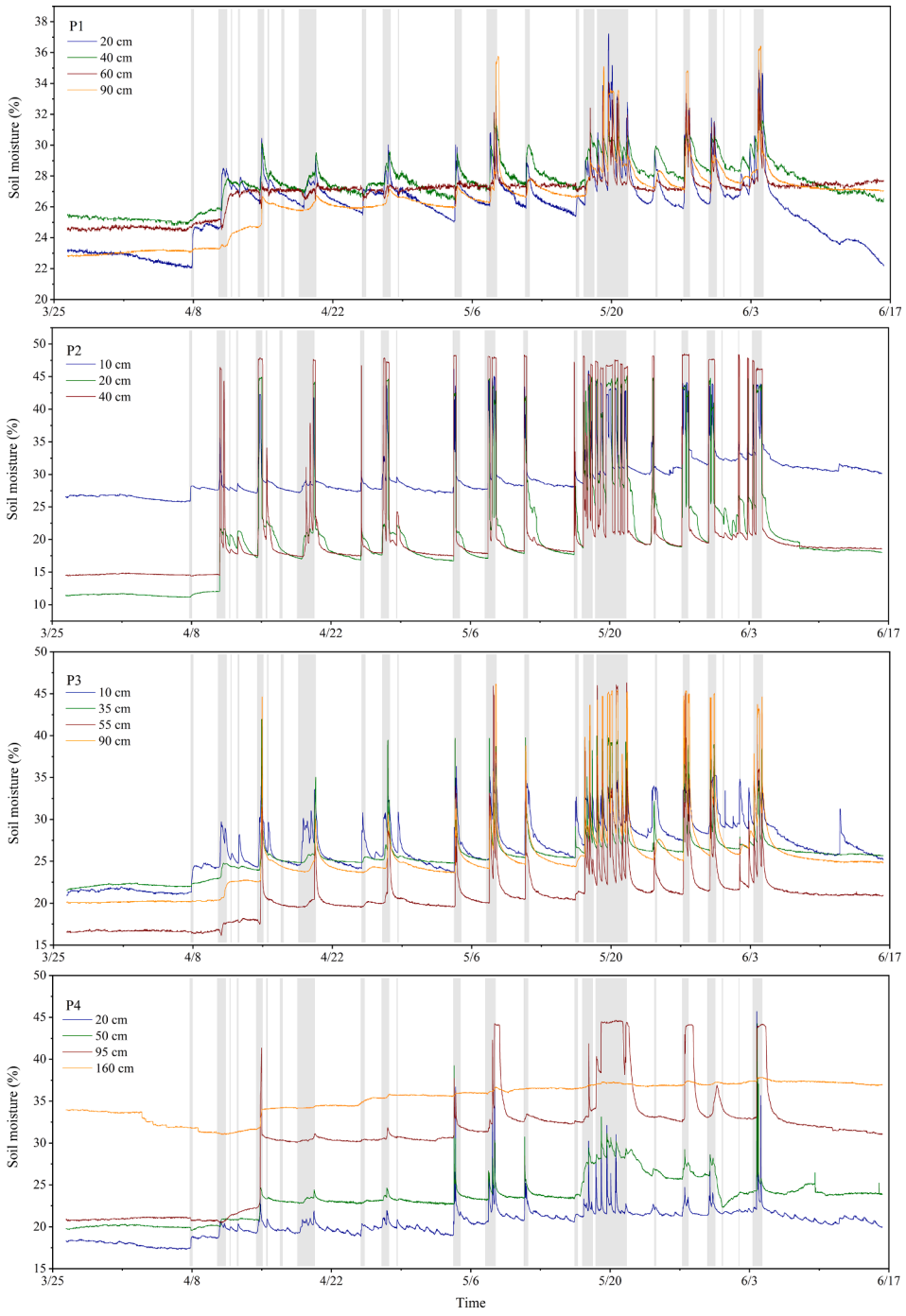

Fig. 3. The time series curve of soil moisture content in soil pits (P1-P4) of HRS-1. The shaded parts indicate rainfall events.

2.4. Hydrological connectivity analysis

A highly permeable soil surface contributes to a large amount of rainfall infiltration, which allows for the development of saturation above an impeding layer (e.g., the interface of soil and bedrock). The lateral transport of free water in the saturated layer forms the subsurface flow. Thus, the existence of a saturated soil was generally regarded as an indication of subsurface flow (van Meerveld et al., 2015). In this study, the hydrological connectivity was analyzed based on the following assumptions: (1) As long as the soil moisture in any soil layer of a zone exceeds its saturation value, we consider subsurface flow has occurred in this zone. (2) When a subsurface flow is established from a zone to the stream, this zone is hydrologically connected to the stream at this moment. However, for example, the midslope and the stream are disconnected when the downslope is not saturated even if subsurface flows are generated in the midslope and riparian zones. (3) We consider that HRS connectivity is established when the downslope is connected to the stream. (4) Preferential flow pathways have the same impacts on the hydrological connectivity of both HRS continuums. The specific HRS connectivity scenarios can be referred to Fig. S2. In this study, the time required to establish hydrological connectivity was calculated according to the difference between the rainfall starting time and the initiation time of HRS connectivity. The connectivity strength characterizing the magnitude of HRS connectivity in rainfall events was estimated as follows:

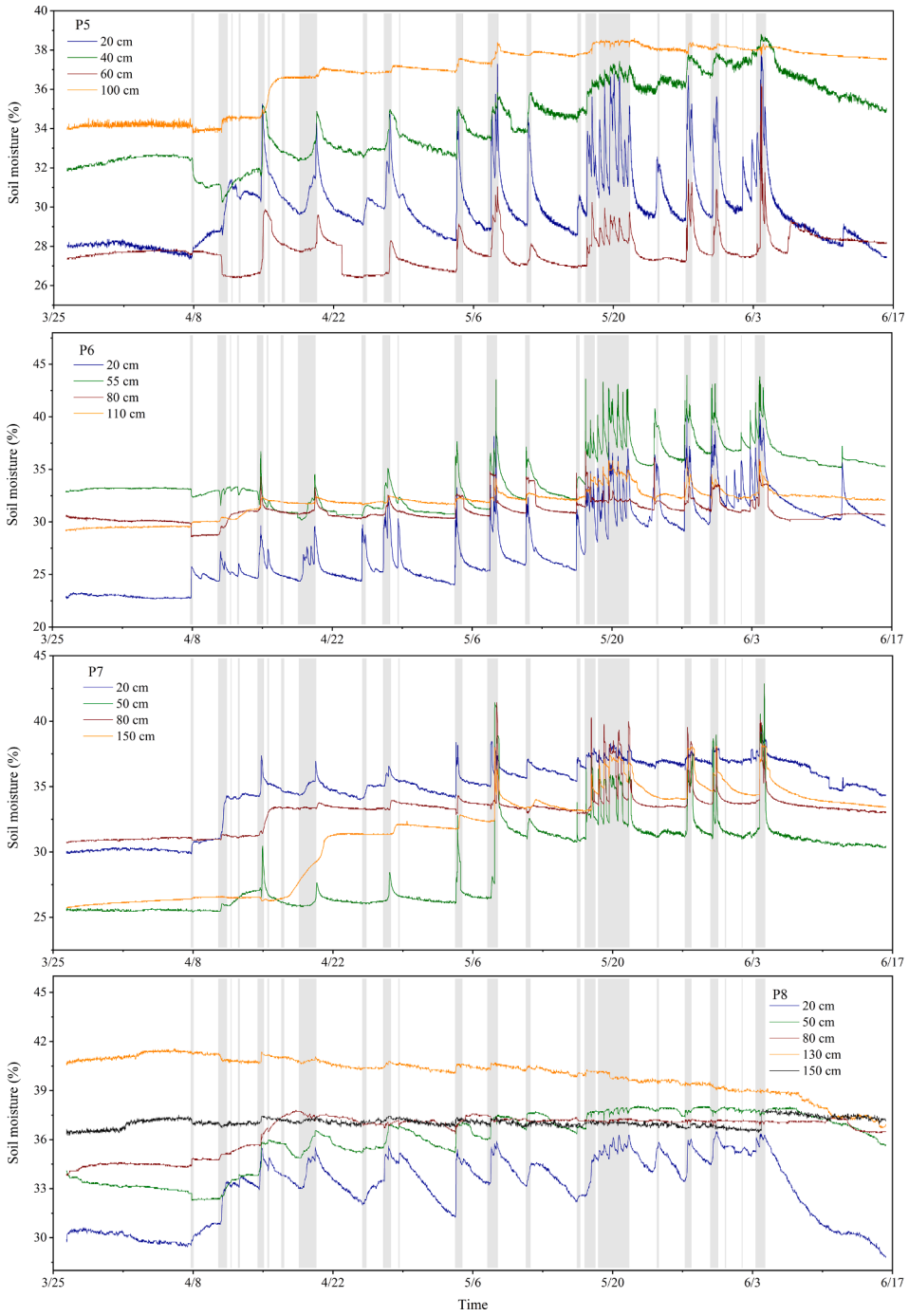

Fig. 4. The time series curve of soil moisture content in different soil pits (P5-P8). The shaded parts indicate rainfall events.

$$Connectivity\ \ strength = \sum w_i (connected\ \ time/duration)_i \quad (2)$$

where *i* indicates the different zones of the hillslope (upslope, midslope and downslope zones); w_i indicates the weight (here, the value is 1/3); *duration* is the time from rain starting to base flow recovery; and *connected time* is the time that a zone is connected to the stream during the *duration*. The value of connectivity strength varies between 0 and 1. The larger the value is, the higher the magnitude of HRS connectivity is.

2.5. Statistical analysis

Partial least squares regression (PLSR) was used to determine the main influencing factors of connectivity strength (dependent variable). The main advantage of this technique is to avoid collinearity problems, permitting working with a number of variables that is greater than the number of samples. To overcome overfitting, the appropriate number of components for the PLSR model was determined by root-mean-square error estimated by cross-validation (RMSECV) to achieve an optimal balance between the explained variation in the response (R^2) and the predictive ability (goodness of prediction, Q^2) (Shi et al., 2014; Iqbal et al., 2013). In the PLSR model, the variable importance of projection (VIP) values were calculated to estimate the importance of the independent variables. The terms with high VIP values were the most relevant in terms of explaining the dependent variable. Detailed information on PLSR algorithms can be found in the relevant literatures (Abdi, 2010; Wu et al., 2010).

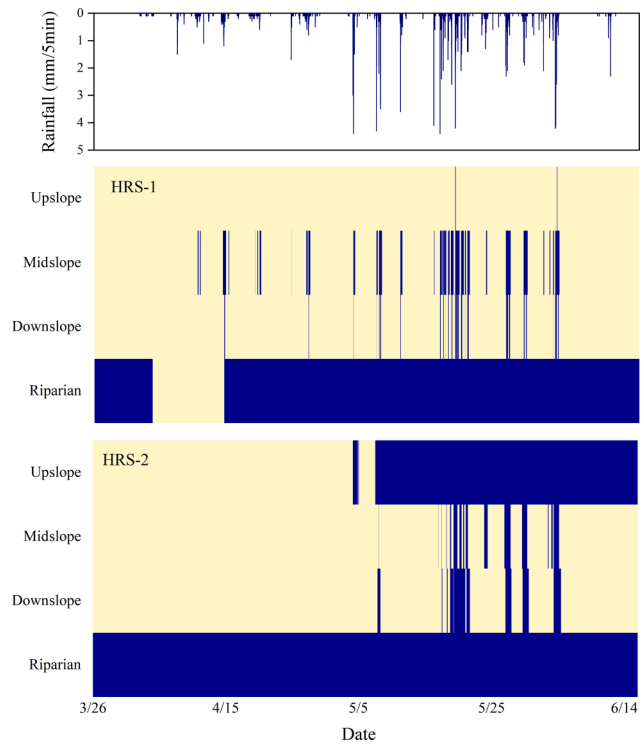

Fig. 5. The spatial and temporal variation of hydrological connectivity in HRS continuums. The yellow color indicates there is no subsurface flow, and the blue color indicates the subsurface flow has been generated. (For interpretation of the references to color in this figure legend, the reader is referred to the web version of this article.)

A clear threshold response of subsurface flow was observed in hillslopes by Tromp-Van Meerveld and McDonnell (2006), and a fill and spill theory was proposed to clarify the threshold behavior. The theory states that subsurface flow is established when bedrock depressions are filled and the water level in these depressions are high enough to start spilling over the bedrock ridges. In this study, the establishment of HRS connectivity was based on subsurface flow, thus we assumed that there is also a threshold response for HRS connectivity. The threshold analysis was conducted between connectivity strength and rainfall amount. The nonlinear relationship between the time required to establish connectivity and I_{30} was analyzed.

3. Results

3.1. The variation in soil moisture

In the HRS-1 continuum, the soil moisture content ranged from 11.14% to 48.55% and showed various response patterns to rainfall in different zones. In the riparian zone (P4), the soil moisture content of the 160 cm soil layer was the largest, followed by that of the 95 cm, 50 cm, and 20 cm soil layers during the non-rainfall period (Fig. 3). A strong increase in soil moisture was observed in the 20 cm, 50 cm, and 95 cm soil layers during rainfall, while no obvious response was observed in the 160 cm soil layer. In the midslope (P2) and downslope (P3) zones, the surface soil moisture (10 cm) was usually higher than that in the deep soil layers (40–90 cm) during the non-rainfall period, and the strongest response of soil moisture to rainfall was observed at the interface of soil and bedrock (at the 40 and 90 cm soil, respectively). For instance, the soil moisture content in the 40 cm soil of the midslope rapidly increased from 17.82% to 48.11% during the rainfall event 3–2. In the upslope zone (P1), the soil moisture varied in a relatively narrow range (from 22.04% to 37.22%), and the response of soil moisture to rainfall in different soil layers was almost consistent (Fig. 3).

Compared with the HRS-1 continuum, the variation range of soil moisture in HRS-2 was relatively narrow, within the range of 22.69% to 43.97%. Similar to the riparian zone of HRS-1 (P4), a stable time series curve for soil moisture was observed in the deep soil layers (130 and 150 cm) in the riparian zone of HRS-2 (P8) (Fig. 4). Furthermore, a weaker response of soil moisture to rainfall was observed in the

Table 3
The characteristics of HRS connectivity under different rainfall events.

Events	HRS-1		HRS-2			
	Time (h) [a]	Upslope connected [b]	Connectivity strength [c]	Time (h)	Upslope connected	Connectivity strength
1–4	0.42	yes	0.175	1.67	yes	0.476
2–1	1.25	yes	0.102	9.17	yes	0.402
3–2	7.50	no	0.044	17.25	yes	0.060
4–5	1.25	no	0.121	4.75	yes	0.323
5–3	1.58	no	0.009	–	no	0
6–10	3.17	no	0.094	14.92	yes	0.031
7–13	10.13	no	0.078	–	no	0
8–14	4.33	no	0.104	6.08	yes	0.526
9–16	–	no	0	–	no	0
10–15	18.58	no	0.020	–	no	0
11–7	1.75	no	0.024	–	no	0
12–22	–	no	0	–	no	0
13–18	–	no	0	–	no	0
14–9	–	no	0	–	no	0
15–6	–	no	0	–	no	0
16–8	–	no	0	–	no	0
17–12	–	no	0	–	no	0
18–11	–	no	0	–	no	0
19–21	–	no	0	–	no	0
20–17	–	no	0	–	no	0
21–23	–	no	0	–	no	0
22–20	–	no	0	–	no	0
23–19	–	no	0	–	no	0
24–24	–	no	0	–	no	0

– indicates no data.
[a] The time required to establish hydrological connectivity.
[b] Whether upslope is connected to the stream.
[c] The hydrological connectivity strength.

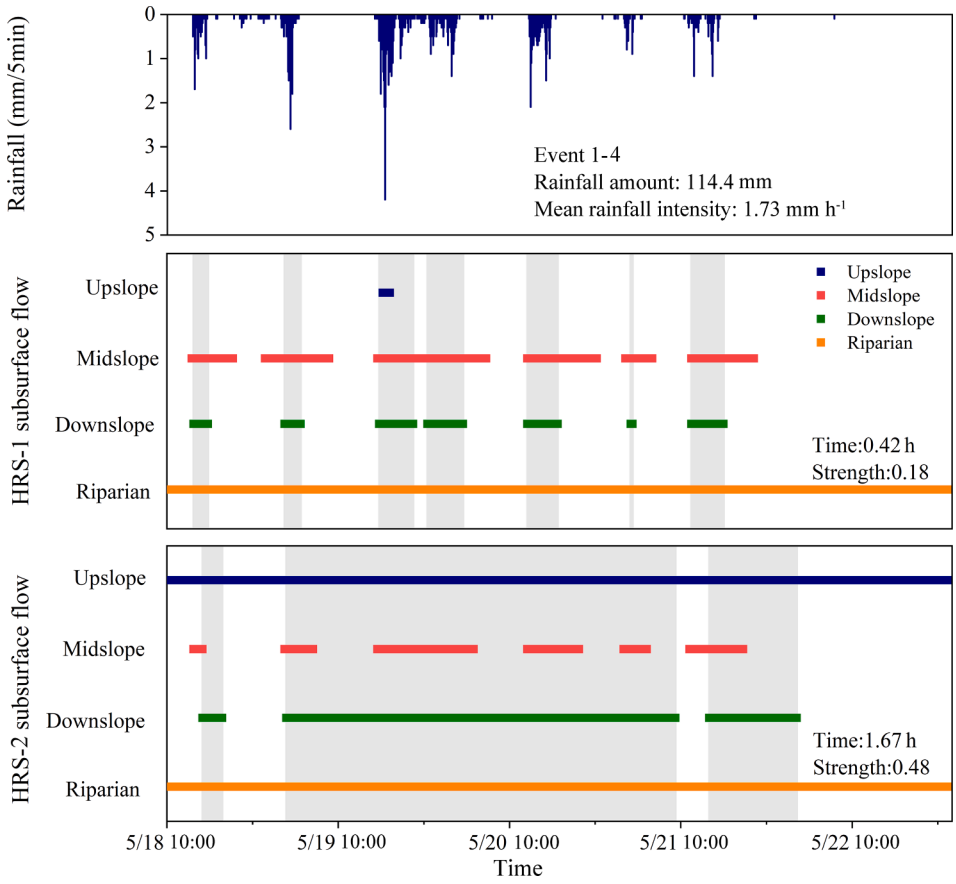

Fig. 6. The subsurface flow and connectivity characteristics of HRS continuums in the rainfall event 1–4. The colored lines indicate subsurface flow has been generated. The shaded parts indicate hydrological connectivity has been established between downslope and the stream. (Time: the time required to establish hydrological connectivity; Strength: the connectivity strength).

midslope and downslope zones of HRS-2 (P6 and P7) than those in the HRS-1. At the upslope of HRS-2 (P5), the soil moisture varied in the range of 26.4% to 38.6% and the overall variation trend was as follows: 100 cm > 40 cm > 20 cm > 60 cm. Furthermore, a stable time series curve of soil moisture was observed in the 100 cm soil layer since the rainfall event 7–14 (Fig. 4).

3.2. The structure influences of HRS connectivity

In the HRS-1 continuum, the riparian zone was connected to the stream during 87% of the monitoring time, while the connection time of the upslope, midslope, and downslope zones accounted for only 0.1%, 3.3%, and 3.3%, respectively, of the monitoring time (Fig. 5). In the HRS-2 continuum, the connection times of the upslope, midslope, downslope, and riparian zones accounted for 4.5%, 4.5%, 7.8%, and 100% of the monitoring time, respectively. Compared with HRS-1, HRS-2 had a longer connectivity time (Fig. 5). HRS connectivity was observed only in 10 and 6 of the 24 rainfall events for the HRS-1 and HRS-2 continuums, respectively. There were only 2 rainfall events (1–4 and 2–1) that connected the upslope of HRS-1 to the stream (Fig. 5 and Table 2). The time required to establish hydrological connectivity in HRS-1 and HRS-2 ranged from 0.42 h to 18.58 h and 1.67 h to 17.25 h, respectively. The required time in HRS-2 was greater than that in HRS-1 in all rainfall events during which HRS-2 established connectivity (Table 3). The connectivity strength of HRS-1 and HRS-2 varied in the range of 0–0.175 and 0–0.526, respectively. In the events with the top four rainfall amounts (1–4, 2–1, 3–2, and 4–5), the connectivity strength in HRS-2 was strongly higher than that in HRS-1. However, in the rainfall event 6–10, lower connectivity strength was observed in HRS-2 (Table 3).

We further elucidated the HRS connectivity in detail through two rainfall events (1–4 and 6–10). Event 1–4 was a heavy-intensity, high-size (114.4 mm) event with a wet antecedent condition. Fig. 6 shows that HRS-1 quickly established hydrological connectivity between the hillslope and stream during the event (the time required to establish HRS connectivity was 0.42 h) and could be disconnected rapidly when the rainfall stopped (approximately 0.5 h). In contrast, the required time in HRS-2 was relatively long (1.67 h), while the subsurface flow could be maintained for a long time after the rainfall cessation (approximately 10.5 h). Event 6–10 was a moderate-intensity, median-size (27.6 mm) event with a dry antecedent condition. In this event, the time required to establish hydrological connectivity in HRS-2 (14.92 h) was also higher than that in HRS-1 (3.16 h) (Fig. 7). However, the hydrological connectivity was maintained for only 2.5 h in HRS-2. The connectivity strength in HRS-2 (0.03) was lower than that in HRS-1 (0.09), which was contrary to event 1–4.

3.3. The rainfall controls of HRS connectivity

A summary of the PLSR model constructed for connectivity strength is presented in Table 4. The minimum RMSECV value (0.032) and the highest Q^2_{cum} value (0.60) were obtained in the first two components of the PLSR model, suggesting that the subsequent components were not strongly correlated with the residuals of the predicted variable. The optimal PLSR model showed that the first component accounted for 64.1% of the variance in connectivity strength. When a second component was added, the model explained 70.5% of the variance (Table 4). However, no improvement in variance was recorded when more components were added to the model. In the PLSR model, only some factors had VIP > 1, including rainfall amount (VIP = 1.60), I_{30} (VIP = 1.27), I_{15}

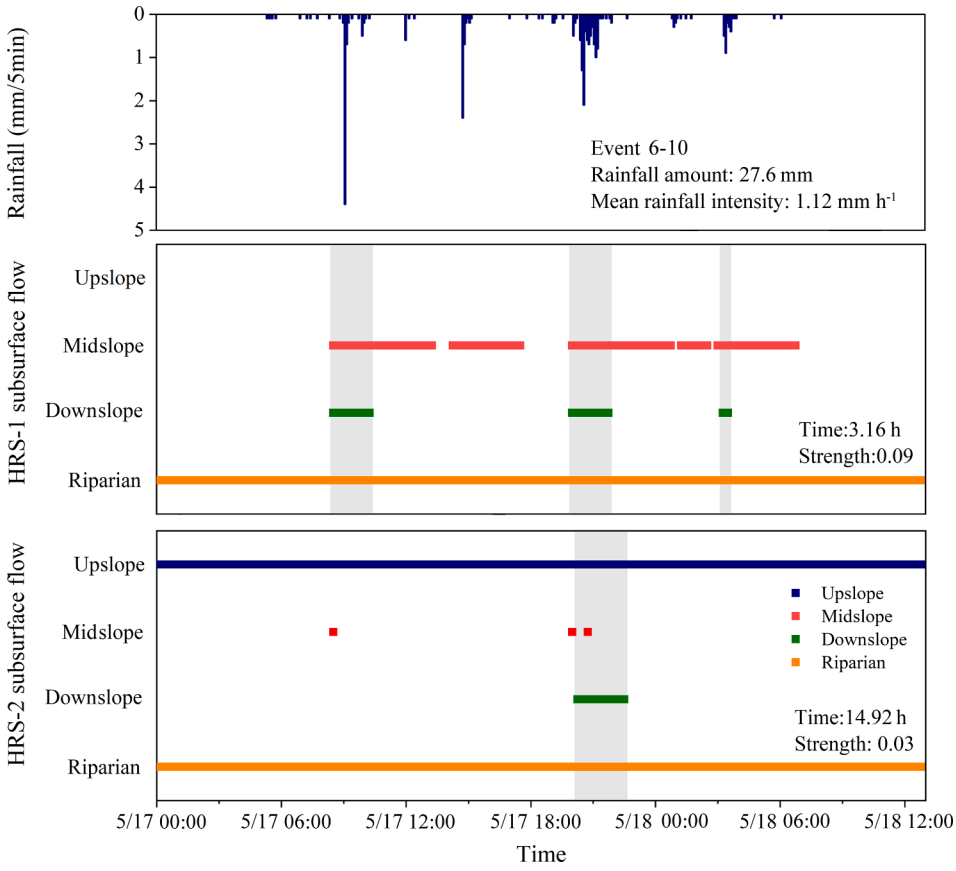

Fig. 7. The subsurface flow and connectivity characteristics of HRS continuums in the rainfall event 6–10. The colored lines indicate subsurface flow has been generated. The shaded parts indicate hydrological connectivity has been established between downslope and the stream. (Time: the time required to establish hydrological connectivity; Strength: the connectivity strength).

Table 4
Summary of the partial least squares regression (PLSR) model for connectivity strength.

Response variable	R^2	Q^2	Component	Explained variability (%)	Cumulative explained variability (%)	RMSECV	Q^2_{cum}
Connectivity strength	0.71	0.60	1	64.1	64.1	0.038	0.581
			2	6.3	70.5	0.032	0.603
			3	2.2	72.7	0.034	0.563
			4	0.9	73.6	0.039	0.520

R^2 indicates the determination coefficient; Q^2 represents the goodness of prediction; RMSECV is root-mean-square error estimated by cross-validation.

(VIP = 1.21), and rainfall duration (VIP = 1.12) (Fig. 8). The lower VIP values for I_{mean}, ASI, and API suggested that the contribution of these factors to connectivity strength was not significant compared to contribution of the others. Furthermore, there was a clear rainfall threshold for HRS connectivity. When the rainfall amount was less than 14.8 mm, HRS-1 did not establish hydrological connectivity during any rainfall event. Conversely, when the rainfall amount exceeded this threshold, the connectivity strength increased with rainfall amount (Fig. 9). In comparison, the rainfall threshold was increased to 21.1 mm in HRS-2. Furthermore, there was a power function relationship between the time required to establish hydrological connectivity and I_{30} in HRS-1. As I_{30} increased, the required time declined remarkably (Fig. 9). However, it is difficult to analyze the relationship between them in HRS-2 as fewer events established HRS connectivity.

4. Discussion

In this study, we monitored soil moisture from the soil surface to the soil–bedrock interface in two HRS continuums with different physical structures (HRS-1: thin soil depth and steep slope; HRS-2: thick soil depth and gentle slope, see Table 1) to reveal the variation in HRS connectivity and its structure and rainfall controls. Similar to the study of Kim (2014), we assumed that the existence of a saturated soil is an indication of subsurface flow. A zone was considered to be hydrologically connected to the stream when subsurface flow was established from that zone to the stream (Stieglitz et al., 2003). We found that the connectivity time accounted for 87% and 100% of the monitoring time for the riparian zone in HRS-1 and HRS-2, respectively. Even in the non-rainfall period, the riparian zone was hydrologically connected to the stream. This result was further verified by our field runoff monitoring, that is, runoff could be always observed at the outlet of the subcatchment during non-rainfall periods (Fig. S3). In contrast, the hydrological connectivity of upslope, midslope, and downslope zones to the stream was observed only during the rainfall period, indicating that rainfall was the prerequisite to establish hydrological connectivity between the hillslope and stream. Furthermore, our analysis revealed that the hydrological connectivity between the hillslope and stream could be established for a longer time for the HRS continuum with a thicker soil depth and gentler slope. Changes in physical structure had a strong impact on the HRS connectivity time.

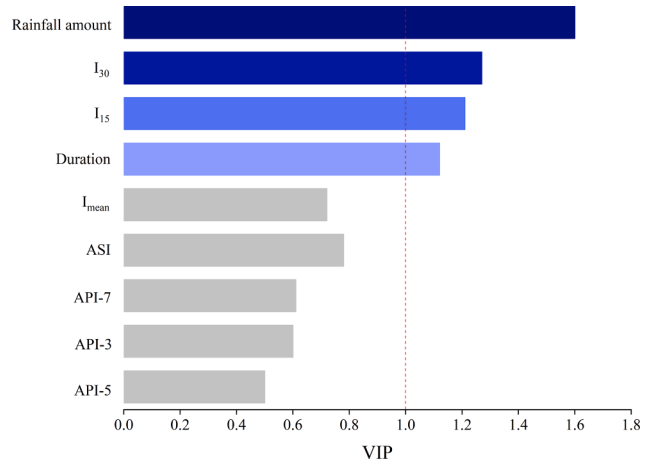

Fig. 8. Variable importance of the projection (VIP) of each predictor of connectivity strength. The red dotted line indicates the threshold above which predictors are considered to be important for interpretation. The abbreviations for the rainfall-related variables are listed in Table 2. (For interpretation of the references to color in this figure legend, the reader is referred to the web version of this article.)

A total of 24 rainfall events were recorded during the monitoring period, while hydrological connectivity between the hillslope and stream was observed only in 10 and 6 rainfall events for the HRS-1 and HRS-2 continuums, respectively. This result indicated that there indeed exist a rainfall threshold for HRS connectivity, and the rainfall threshold in HRS-2 is likely higher than that in HRS-1. By analyzing the time required to establish hydrological connectivity for each rainfall event, we found that the required time for connectivity initiation in HRS-1 was lower than that in HRS-2, which supported our first hypothesis (H1) that hydrological connectivity could be established quickly in the HRS continuum with a steeper slope and thinner soil depth. According to the study of Han et al. (2020), approximately 90% HRS connectivity were established through saturation connectivity initiating at the soil–bedrock interface. The infiltration of rainfall from the surface to the bedrock has strong impact on the required time (Miyata et al., 2019). Thin soil depths generally have limited water storage capacity (Peterman et al., 2014), and rainfall can quickly infiltrate from the surface to the bedrock (Ocampo et al., 2006). A steep slope can accelerate the lateral transport of water in the saturated layer, forming continuous subsurface flow (Blume et al., 2009). Thus, the time required to establish connectivity was decreased in the HRS-1 continuum. Based on the above findings, we can infer that the contribution of various HRS continuums to runoff may be different during a rainfall event. At the early stage of a rainstorm, the runoff and solutes in the stream may mainly come from the HRS continuums with thin soil depths and steep slopes as they are

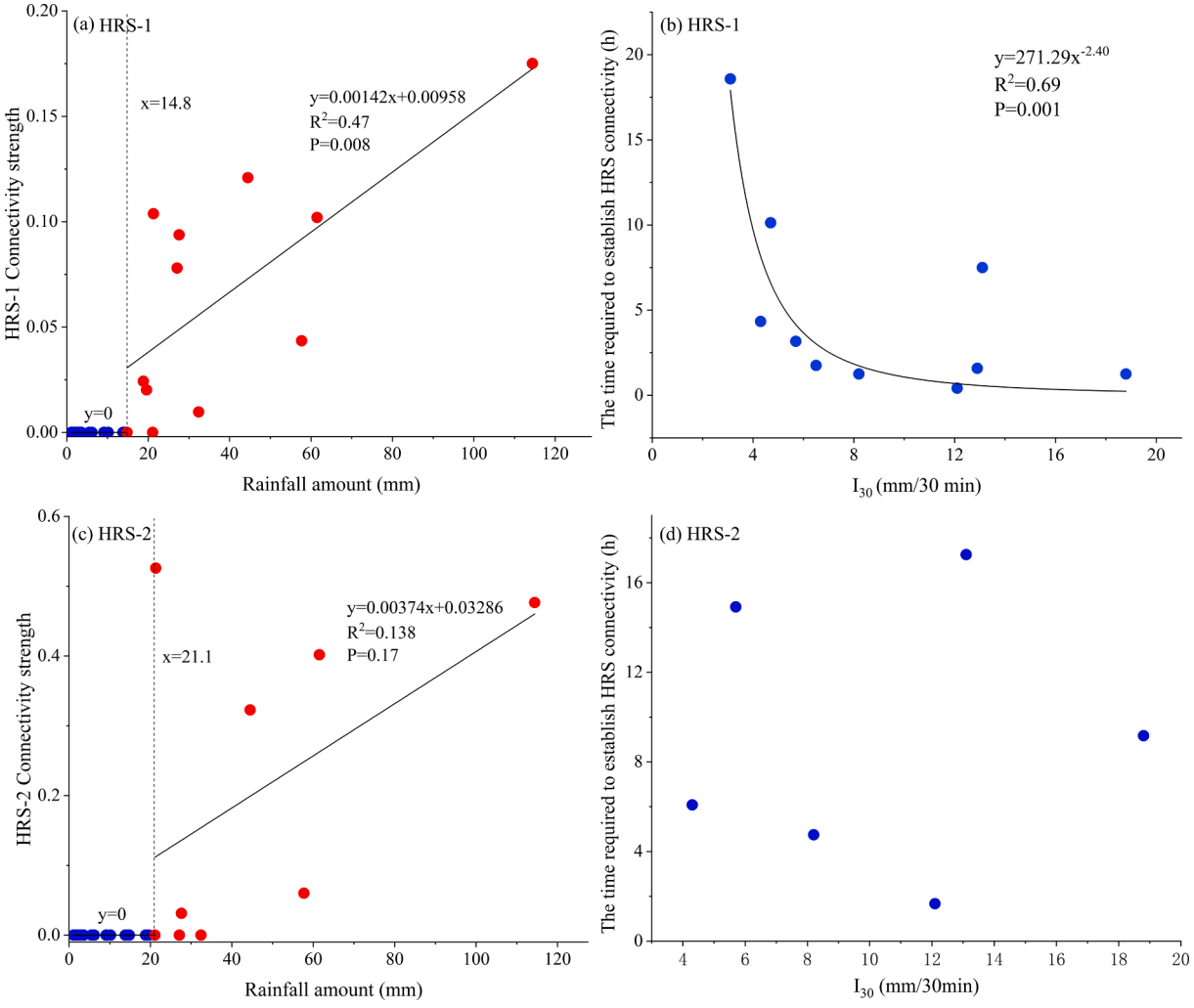

Fig. 9. The relationships between connectivity strength and rainfall amount (a, c), and between the time required to establish hydrological connectivity and 30 min maximum rainfall intensity (I_{30}) (b, d).

the first to establish connection with stream. Then, the runoff source area gradually expands to the HRS continuums with thick soil and gentle slopes. By analyzing the HRS connectivity in detail in event 1–4, we found that the downslope of HRS-1 was disconnected with stream quickly after rainfall cessation, while the connectivity was maintained for a long time between them in HRS-2. For heavy rainfall events, thus, hillslopes with thick soil and gentle slopes may be the main contributors to runoff during the period from rainfall cessation to base flow recovery. In contrast, the connectivity of HRS-2 was maintained for only 2.5 h in the event 6–10. The short connectivity time of HRS-2 indicated that the contribution of an HRS continuum with a deep soil and gentle slope to runoff may be limited in moderate rainfall events.

Our analysis also revealed that the peak rainfall intensity was the main control affecting the time required to establish hydrological connectivity in the HRS-1 continuum. As rainfall intensified, the time required to generate connectivity shortened exponentially. This finding was consistent with the study of Han et al. (2020) who examined different HRS connectivity patterns in a steep forested catchment and indicated that peak rainfall intensity determined the initiation of connectivity. In high-intensity rainfall events, the saturation connectivity between soil horizons (SCSH) can be established by rapidly generating perched water tables. However, saturation connectivity that initiates at the soil–bedrock interface (SCSB) is likely the main connectivity pattern for moderate-intensity rainfall events, and the time required to establish the SCSH is generally shorter than that of the SCSB (Han et al., 2020). Thus, the variations in connectivity patterns induced by peak rainfall intensity have a strong impact on the time required to establish HRS connectivity, and the required time is markedly reduced with the increase in peak rainfall intensity. In addition, variation in the required time with peak rainfall intensity can be further explained by the fill and spill theory (Bracken et al., 2013), which states that subsurface stormflow is established when bedrock depressions are filled and the water level in these depressions are high enough to start spilling over the bedrock ridges (Tromp-Van Meerveld and McDonnell, 2006). Increase in rainfall intensity can decrease the filling time of bedrock depressions rapidly, thus the required time for initiating connectivity is shortened.

The variations in HRS physical structure strongly influenced the connectivity strength, and the HRS continuum with a thicker soil depth and gentler slope exhibited higher connectivity strength during heavy rainfall events (1–4, 2–1, 3–2 and 4–5). The differences in connectivity time and spatial expansion extent may be the main reasons for the large discrepancy in the connectivity strength between HRS continuums (Wang et al., 2014). In heavy rainfall events, the high connectivity time and subsurface flow expansion extent led to increased connectivity strength in the HRS-2 continuum. For instance, in event 1–4, the connectivity time of the midslope accounted for 25.6% and 35.0% of the duration from rainfall starting to base flow recovery for the HRS-1 and HRS-2 continuums, respectively. The results of the PLSR model indicated that rainfall amount, I_{30}, I_{15}, and duration were the important influencing factors for connectivity strength. Compared with the ASI and API, the rainfall amount and peak rainfall intensity exerted stronger influences on the connectivity strength, which was inconsistent with the studies of Kampf (2011) and Moreno-de-las-Heras et al. (2020). For instance, Moreno-de-las-Heras et al. (2020) examined the structural and functional controls of surface-patch to hillslope-scale runoff and sediment connectivity and indicated that event-based runoff connectivity was dramatically controlled by antecedent wet conditions and rainfall intensity. Castillo et al. (2003) noted that antecedent soil water was an important factor in controlling runoff during medium- and low-intensity storms. In our study, the hydrometric monitoring was mainly concentrated in the rainy season (from March to June). The intensive rainfall events during the monitoring period resulted in the antecedent soil moisture keeping a steady high value (see ASI-P3 and ASI-P7 in Table 2), which might mask the effect of antecedent soil moisture (Penna et al., 2011; Tromp-Van Meerveld and McDonnell, 2006). In future studies, it is necessary to compare the variations in HRS connectivity between rainy and dry seasons to further reveal the influence mechanisms of antecedent soil moisture on hydrological connectivity.

By further analyzing the relationship between connectivity strength and rainfall amount, we found that the rainfall amount had a clear threshold effect on connectivity strength, which was consistent with our second hypothesis (H2). When the rainfall amount was less than 14.8 mm, HRS-1 did not establish hydrological connectivity during any rainfall event. However, a positive relationship was observed between them when the rainfall exceeded this threshold. In the HRS-2, the threshold was increased to 21.1 mm. These results revealed that the rainfall threshold was closely related to the HRS physical structure. As the soil depth increased and the slope decreased, the rainfall threshold for HRS connectivity increased. Based on these findings, it can be inferred that the main runoff source area of the catchment may exhibit a strong discrepancy among different rainfall events. In slight and moderate rainfall events, such as the event 10–15, runoff may mainly come from HRS continuums with lower rainfall thresholds. With the increase in rainfall amount, the runoff source area of the watershed further expands to the hillslopes of HRS continuums with high rainfall thresholds. These findings further confirmed the theory of variable runoff sources (Costa et al., 2020; Kuo et al., 1999; Lee and Delleur, 1976). We believe that the physical structure and rainfall controls on HRS connectivity revealed in this study will provide a better understanding of runoff generation and solute transport.

5. Conclusion

This study revealed that changes in physical structure and rainfall could strongly influence HRS connectivity. The time required to establish hydrological connectivity was lower in the HRS continuum with a thinner soil depth and steeper slope, which indicated that the contribution to runoff of these HRS continuums was dominant at the early stage of the rainstorm. As rainfall intensified, the required time was shortened exponentially due to the changes in connectivity patterns. Higher connectivity strength was observed in the HRS continuums with a thicker soil depth and gentler slope during heavy rainfall events, and these HRS continuums were the main runoff source areas during the period from rain cessation to base flow recovery. The PLSR analysis showed that rainfall amount, I_{30}, I_{15}, and rainfall duration were the dominant rainfall controls affecting connectivity strength. Compared with antecedent soil moisture, the rainfall amount and peak rainfall intensity exerted more important regulatory effects on the connectivity strength during the rainy season. Furthermore, there was a clear rainfall threshold for HRS connectivity. When the rainfall amount exceeded the threshold, a positive relationship was observed between connectivity strength and rainfall amount. Furthermore, the threshold varied from 14.8 mm in HRS-1 to 21.1 mm in HRS-2. Our results suggested that the physical structure of the HRS exerts a primary control on the rainfall threshold.

Declaration of Competing Interest

The authors declare that they have no known competing financial interests or personal relationships that could have appeared to influence the work reported in this paper.

Acknowledgements

Financial support for this research was provided by the National Natural Science Foundation of China (Grant No. 41930755, 42007059), the Strategic Priority Research Program of Chinese Academy of Sciences (Grant No. XDB 40000000), the Open Research Fund of the Key Laboratory of Soil Erosion and Prevention in Jiangxi Province (Grant No. 2021SKTR01), and the China Postdoctoral Science Foundation (2019M662669).

Appendix A. Supplementary material

Supplementary data to this article can be found online at https://doi.org/10.1016/j.catena.2022.106286.

References

Abdi, H., 2010. Partial least squares regression and projection on latent structure regression (PLS Regression). WIREs Comp. Stat. 2 (1), 97–106.

Blume, T., Zehe, E., Bronstert, A., 2009. Use of soil moisture dynamics and patterns at different spatio-temporal scales for the investigation of subsurface flow processes. Hydrol. Earth Syst. Sci. 13, 1215–1233.

Blume, T., van Meerveld, H.J.(Ilja), 2015. From hillslope to stream: methods to investigate subsurface connectivity. WIREs Water 2, 177–198.

Bracken, L.J., Wainwright, J., Ali, G.A., Tetzlaff, D., Smith, M.W., Reaney, S.M., Roy, A. G., 2013. Concepts of hydrological connectivity: Research approaches, pathways and future agendas. Earth Sci. Rev. 119, 17–34.

Burns, M.A., Barnard, H.R., Gabor, R.S., McKnight, D.M., Brooks, P.D., 2016. Dissolved organic matter transport reflects hillslope to stream connectivity during snowmelt in a montane catchment. Water Resour. Res. 52 (6), 4905–4923.

Cartwright, I., Morgenstern, U., 2018. Using tritium and other geochemical tracers to address the "old water paradox" in headwater catchments. J. Hydrol. 563, 13–21.

Castillo, V., Gomezplaza, A., Martinezmena, M., 2003. The role of antecedent soil water content in the runoff response of semiarid catchments: A simulation approach. J. Hydrol. 284 (1-4), 114–130.

Costa, D., Shook, K., Spence, C., Elliott, J., Baulch, H., Wilson, H., Pomeroy, J.W., 2020. Predicting variable contributing areas, hydrological connectivity, and solute transport pathways for a Canadian prairie basin. Water Resour. Res. 56, e2020WR027984.

Detty, J.M., McGuire, K.J., 2010. Topographic controls on shallow groundwater dynamics: Implications of hydrologic connectivity between hillslopes and riparian zones in a till mantled catchment. Hydrol. Process. 24, 2222–2236.

Farrick, K.K., Branfireun, B.A., 2014. Soil water storage, rainfall and runoff relationships in a tropical dry forest catchment. Water Resour. Res. 50 (12), 9236–9250.

Fiori, A., Russo, D., 2007. Numerical analyses of subsurface flow in a steep hillslope under rainfall: The role of the spatial heterogeneity of the formation hydraulic properties. Water Resour. Res. 43, W07445.

Fu, C., Chen, J., Jiang, H., Dong, L., 2013. Threshold behavior in a fissured granitic catchment in southern China: 1. Analysis of field monitoring results. Water Resour. Res. 49 (5), 2519–2535.

Garvelmann, J., Külls, C., Weiler, M., 2012. A porewater-based stable isotope approach for the investigation of subsurface hydrological processes. Hydrol. Earth Syst. Sci. 16, 631–640.

Gish, T.J., Walthall, C.L., Daughtry, C.S.T., Kung, K.-J.- S., 2005. Using soil moisture and spatial yield patterns to identify subsurface flow pathways. J. Hydrol. 34 (1), 274–286.

Hagedorn, F., Schleppi, P., Waldner, P., Flühler, H., 2000. Export of dissolved organic carbon and nitrogen from Gleysol dominated catchments – the significance of water flow paths. Biogeochemistry 50, 137–161.

Han, X., Liu, J., Srivastava, P., Mitra, S., He, R., 2020. Effects of critical zone structure on patterns of flow connectivity induced by rainstorms in a steep forested catchment. J. Hydrol. 587, 125032.

Hopp, L., McDonnell, J.J., 2009. Connectivity at the hillslope scale: Identifying interactions between storm size, bedrock permeability, slope angle and soil depth. J. Hydrol. 376 (3-4), 378–391.

Ilek, A., Kucza, J., Szostek, M., 2017. The effect of the bulk density and the decomposition index of organic matter on the water storage capacity of the surface layers of forest soils. Geoderma 285, 27–34.

Iqbal, A., Sun, D.-W., Allen, P., 2013. Prediction of moisture, color and pH in cooked, pre-sliced turkey hams by NIR hyperspectral imaging system. J. Food Eng. 117 (1), 42–51.

Jencso, K.G., McGlynn, B.L., Gooseff, M.N., Wondzell, S.M., Bencala, K.E., Marshall, L.A., 2009. Hydrologic connectivity between landscapes and streams: Transferring reach- and plot-scale understanding to the catchment scale. Water Resour. Res. 45, 1–16.

Jia, J., Gao, Y., 2017. Acid deposition and assessment of its critical load for the environmental health of waterbodies in a subtropical watershed. China. J. Hydrol. 555, 155–168.

Kampf, S.K., 2011. Variability and persistence of hillslope initial conditions: A continuous perspective on subsurface flow response to rain events. J. Hydrol. 404 (3-4), 176–185.

Kim, S., 2014. Connectivity and topographic thresholds in bi-hourly soil moisture measurements along transects on a steep hillslope. J. Hydrol. 512, 563–574.

Kuo, W.-L., Steenhuis, T.S., McCulloch, C.E., Mohler, C.L., Weinstein, D.A., DeGloria, S. D., Swaney, D.P., 1999. Effect of grid size on runoff and soil moisture for a variable-source-area hydrology model. Water Resour. Res. 35 (11), 3419–3428.

Lee, M.T., Delleur, J.W., 1976. A variable source area model of the rainfall-runoff process based on the Watershed Stream Network. Water Resour. Res. 12 (5), 1029–1036.

McGuire, K.J., McDonnell, J.J., 2010. Hydrological connectivity of hillslopes and streams: Characteristic time scales and nonlinearities. Water Resour. Res. 46, 1–17.

Miyata, S., Gomi, T., Sidle, R.C., Hiraoka, M., Onda, Y., Yamamoto, K., Nonoda, T., 2019. Assessing spatially distributed infiltration capacity to evaluate storm runoff in forested catchments: Implications for hydrological connectivity. Sci. Total Environ. 669, 148–159.

Moreno-De-Las-Heras, M., Merino-Martín, L., Saco, P.M., Espigares, T., Gallart, F., Nicolau, J.M., 2020. Structural and functional control of surface-patch to hillslope runoff and sediment connectivity in Mediterranean dry reclaimed slope systems. Hydrol. Earth Syst. Sci. 24, 2855–2872.

Nanda, A., Sen, S., McNamara, J.P., 2019. How spatiotemporal variation of soil moisture can explain hydrological connectivity of infiltration-excess dominated hillslope: Observations from lesser Himalayan landscape. J. Hydrol. 579, 124146.

Ocampo, C.J., Sivapalan, M., Oldham, C., 2006. Hydrological connectivity of upland-riparian zones in agricultural catchments: Implications for runoff generation and nitrate transport. J. Hydrol. 331 (3-4), 643–658.

Onda, Y., Komatsu, Y., Tsujimura, M., Fujihara, J.-I., 2001. The role of subsurface runoff through bedrock on storm flow generation. Hydrol. Process. 15 (10), 1693–1706.

Outram, F.N., Cooper, R.J., Sünnenberg, G., Hiscock, K.M., Lovett, A.A., 2016. Antecedent conditions, hydrological connectivity and anthropogenic inputs: Factors affecting nitrate and phosphorus transfers to agricultural headwater streams. Sci. Total Environ. 545–546, 184–199.

Penna, D., Tromp-Van Meerveld, H.J., Gobbi, A., Borga, M., Dalla Fontana, G., 2011. The influence of soil moisture on threshold runoff generation processes in an alpine headwater catchment. Hydrol. Earth Syst. Sci. 15, 689–702.

Peterman, W., Bachelet, D., Ferschweiler, K., Sheehan, T., 2014. Soil depth affects simulated carbon and water in the MC2 dynamic global vegetation model. Ecol. Model. 294, 84–93.

Rinderer, M., Meerveld, H.J., McGlynn, B.L., 2019. From points to patterns: Using groundwater time series clustering to investigate subsurface hydrological connectivity and runoff source area dynamics. Water Resour. Res. 55 (7), 5784–5806.

Shi, Z.H., Huang, X.D., Ai, L., Fang, N.F., Wu, G.L., 2014. Quantitative analysis of factors controlling sediment yield in mountainous watersheds. Geomorphology 226, 193–201.

Stieglitz, M., Shaman, J., McNamara, J., Engel, V., Shanley, J., Kling, G.W., 2003. An approach to understanding hydrologic connectivity on the hillslope and the implications for nutrient transport. Global Biogeochem. Cy. 17 (4), n/a–n/a.

Strohmeier, S., Knorr, K.H., Reichert, M., Frei, S., Fleckenstein, J.H., Peiffer, S., Matzner, E., 2013. Concentrations and fluxes of dissolved organic carbon in runoff from a forested catchment: Insights from high frequency measurements. Biogeosciences 10, 905–916.

Tromp-Van Meerveld, H.J., McDonnell, J.J., 2006. Threshold relations in subsurface stormflow: 1. A 147-storm analysis of the Panola hillslope. Water Resour. Res. 42, 1–11.

van Meerveld, H.J., Seibert, J., Peters, N.E., 2015. Hillslope-riparian-stream connectivity and flow directions at the Panola Mountain Research Watershed. Hydrol. Process. 29, 3556–3574.

van Verseveld, W.J., McDonnell, J.J., Lajtha, K., 2009. The role of hillslope hydrology in controlling nutrient loss. J. Hydrol. 367 (3-4), 177–187.

Wang, H.E., Bénar, C.G., Quilichini, P.P., Friston, K.J., Jirsa, V.K., Bernard, C., 2014. A systematic framework for functional connectivity measures. Front, Neurosci, p. 8.

Weiler, M., Naef, F., 2003. An experimental tracer study of the role of macropores in infiltration in grassland soils. Hydrol. Process. 17 (2), 477–493.

Wu, Z., Li, D., Meng, J., Wang, H., 2010. Introduction to SIMCA-P and Its Application. In: Esposito Vinzi, V., Chin, W., Henseler, J., Wang, H. (Eds.), Handbook of Partial Least Squares. Springer Handbooks of Computational Statistics, Springer, Berlin, Heidelberg.

Yang, L., Wei, W., Chen, L., Chen, W., Wang, J., 2014. Response of temporal variation of soil moisture to vegetation restoration in semi-arid Loess Plateau, China. Catena 115, 123–133.

Yu, H., Yang, P., Lin, H., Ren, S., He, X., 2014. Effects of sodic soil reclamation using flue gas desulphurization gypsum on soil pore characteristics, bulk density, and saturated hydraulic conductivity. Soil Sci. Soc. Am. J. 78 (4), 1201–1213.

Zhao, G., Gao, Y., Wang, L., Hao, Z., Wen, X., Song, X., 2019. Isotopically-tracked hydrological changes in carbon cycling and its sources in a Chinese subtropical forested watershed. J. Hydrol. 575, 1041–1051.

Zuecco, G., Rinderer, M., Penna, D., Borga, M., van Meerveld, H.J., 2019. Quantification of subsurface hydrologic connectivity in four headwater catchments using graph theory. Sci. Total Environ. 646, 1265–1280.